

The excitation function for $\text{Li}+\text{HF}\rightarrow\text{LiF}+\text{H}$ at collision energies below 80 meV

Rolf Bobbenkamp*, Hansjürgen Loesch
Fakultät für Physik, Universität Bielefeld, 33501 Bielefeld, Germany

Marcel Mudrich, Frank Stienkemeier
Physikalisches Institut, Universität Freiburg, 79104 Freiburg, Germany

We have measured the dependence of the relative integral cross section of the reaction $\text{Li}+\text{HF}\rightarrow\text{LiF}+\text{H}$ on the collision energy using crossed molecular beams. By varying the intersection angle of the beams from 37° to 90° we covered the energy range $25\text{ meV}\leq E_{\text{tr}}\leq 131\text{ meV}$. We observe a monotonous rise of the cross section with decreasing energy over the entire energy range indicating that a possible translational energy threshold to the reaction is significantly smaller than 25 meV. The steep rise is quantitatively recovered by a Langevin-type excitation function based on a vanishing threshold and a mean interaction potential energy $\propto R^{-2.5}$ where R is the distance between the reactants. To date all threshold energies deduced from *ab-initio* potentials and zero-point vibrational energies are at variance with our results, however, our findings support recent quantum scattering calculations that predict significant product formation at collision energies far below these theoretical thresholds.

I. INTRODUCTION

The rapid development of techniques for cooling, trapping and manipulating cold and ultracold molecules opens the opportunity of studying chemical reactivity in the low temperature regime [1–4]. Cold reactive collisions are not only important limitations to stable trapping of molecules but also present fascinating aspects of their own interest. In the cold collision regime, reactions are governed by quantum dynamics involving tunneling and scattering resonances [2, 5]. For our study of cold collision phenomena we have selected the title reaction due to both the availability of theoretical results and the applicability of a variety of experimental methods.

Attractive from the theoretical point of view is the small number of electrons together with three chemically very different but light atomic constituents that make the slightly exoergic ($\approx 0.16\text{ meV}$) reaction $\text{Li}+\text{HF}\rightarrow\text{LiF}+\text{H}$ an ideal prototype system for developing methods to calculate reliable *ab-initio* potential energy surfaces (PESs) [6–16] and to calculate quantum scattering phenomena [5, 12, 13, 17–32]. Particularly challenging for a quantitative prediction of observables is the low energy range near threshold where quantum effects dominate and a precise knowledge of the PES around the transition state is essential. Crucial for the assessment of the preciseness and reliability of the applied theoretical methods is the comparison of experimental and computational results. Very qualified for this purpose are certainly angular and velocity distributions of products [15, 33] but also the dependence of the relative integral reaction cross section (IRCS) on the translational collision energy, E_{tr} , the excitation function [22, 26, 30, 34, 35]. At low collision energies the excitation function bears direct information

on the existence and size of a translational threshold that allows a sensitive examination of the shape of the PES near the transition state and the height of a possible potential energy barrier.

An inspection of computational results shows that all PESs [6–16] known to date feature a significant barrier at a bent transition state with substantial height. However including zero point energies of both the reactants and the transition state the semi-classical translational threshold energies deduced from these barrier heights turn out to be markedly smaller. For example, for the most frequently used recent PESs, the semi-classical thresholds and barriers amount to ≈ 27 and 182 meV [12], $\approx 68\text{ meV}$ and 233 meV [13], ≈ 56 and 221 meV [15, 16], respectively. Neglecting quantum scattering phenomena the semi-classical thresholds manifest the lowest collision energies required for product formation from ground state reactants. An observation of products at energies below these calculated thresholds could be a clue to marked quantum phenomena or to insufficient accuracy of the PESs or to a combination of both. Recently, it has been demonstrated in time-dependent wave packet scattering calculations [5, 32] based on the PES of ref. [15, 16] that resonances play an important role for $\text{Li}+\text{HF}$. They lead to product formation at a significant rate at collision energies far below the semi-classical threshold.

One interesting experimental aspect of the title reaction is the availability of methods that allow to investigate scattering phenomena in a wide range of collision energies from hot (several 100 meV) to cold (20 meV) and ultra-cold ($< 1\text{ meV}$). In an earlier experimental study we have measured the excitation function within the range $82\text{ meV}\leq E_{\text{tr}}\leq 376\text{ meV}$ [35] using molecular beams intersecting at a 90° angle. The energy was varied by applying the seeded beam technique. At energies above $\approx 120\text{ meV}$ the function turns out to be roughly constant but below it rises steeply with decreasing E_{tr} and assumes at the lowest energies the largest values within the entire range. Consequently, a threshold to reaction, if existing

*Present address: Carl Zeiss Optronics GmbH, 35576 Wetzlar, Germany

at all, has to be located below 82 meV.

In the present paper we report the results of another crossed beam study on the excitation function designed to lower the range of translational energy to 25 meV. Variation of the collision energy is achieved by varying the intersection angle of the beams (see below). We find that in the extended energy range the IRCS continues to rise monotonously with decreasing E_{tr} thus shifting the upper boundary of a threshold to below 25 meV.

It should be noted that a novel experimental setup using new techniques for preparing samples of cold atoms and molecules is about to be completed. It will allow to continue our search for the threshold of this process at energies below 1 meV.

II. EXPERIMENTAL METHODS

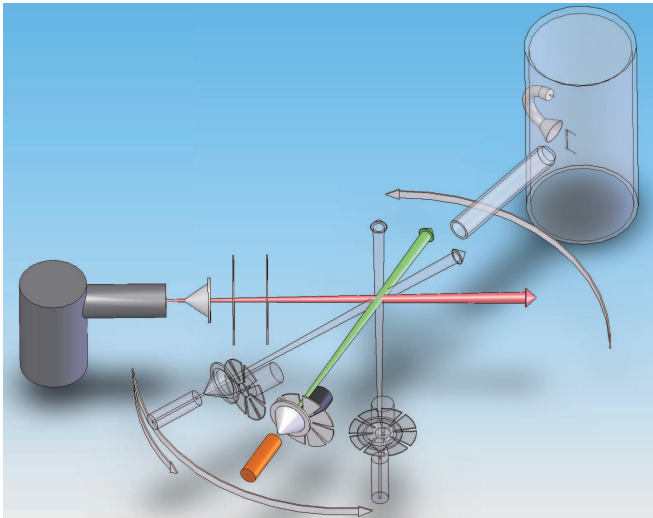


FIG. 1: Schematic view of the molecular beams arrangement. The setup is basically the same as used in our previous experiments [35] except for the HF beam that can now be rotated around the intersection volume to vary the intersection angle Γ in the range $37^\circ \leq \Gamma \leq 90^\circ$. An additional HF-beam modulator placed between nozzle and skimmer is not shown for clarity.

To achieve translational energies below 82 meV (the lowest energy accessible in ref. [35]) we abandon the usual 90° geometry and cross the beams at a variable intersection angle [36–38]. Fig. 1 shows a sketch of the molecular beams arrangement. It deviates from the one used in earlier experimental studies [33, 35, 39] only by the setup of the HF-beam. The nozzle is now mounted within a differentially pumped vacuum chamber (not shown) that can be rotated around the scattering volume. In this way the intersection angle Γ of the two beams and thus also the mean relative velocity

$$\bar{v} = [v_{Li}^2 + v_{HF}^2 - 2v_{Li}v_{HF} \cos \Gamma]^{0.5} \quad (1)$$

TABLE I: Beam velocity parameters, velocities in m/s

Run	u_{Li}	α_{Li}	u_{HF}	α_{HF}
A/B	1530	221	1205	185
C	1750	290	1215	195

and the translational collision energy

$$E_{tr}(\Gamma) = \frac{1}{2}\mu\bar{v}^2 \quad (2)$$

can be varied continuously. μ denotes the reduced mass of the colliding reactants and v_{Li} , v_{HF} are their nominal velocity. Depending on Γ , significantly smaller or larger collision energies can be achieved compared to the one obtained for the usual perpendicular intersection. In this study the two vacuum chambers housing the beam sources are designed such that Γ can be varied in the range $37^\circ \leq \Gamma \leq 90^\circ$.

The experimental method and data acquisition follows closely the ones discussed in ref. [35]. Briefly, the neat HF beam is created by a nozzle heated to around 500 K to avoid clustering. Stagnation pressure (250 mbar) and nozzle temperature are always kept constant. The elevated temperature leads to a mean rotational energy of 8.9 meV [35] and a population of the first vibrationally excited state of $< 0.25\%$. The beam is chopped with a frequency of a few Hz using a tuning-fork like modulator or a chopper wheel at a duty cycle of 50% and the intensity is monitored by a quadrupole mass spectrometer detector equipped with an electron bombardment ion source. The Li beam is diluted with Ne and its intensity is measured by surface ionization on a hot rhenium (Re) ribbon. During an experimental run only the intersection angle Γ is varied while the operational conditions of the beams are kept constant.

The velocity of both beams is determined by conventional time-of-flight (TOF) arrangements. The (density) velocity distributions, $n(v)$, are extracted from the measured TOF profiles by fitting the parameters u , α of the expression

$$n(v) = const v^2 \exp\{-(v-u)/\alpha\}^2 \quad (3)$$

to the data. The parameters u and α of the various data sets are compiled in Table 1. The velocity spreads of the Li and HF beams α result in an experimental relative uncertainty of the collision energy E_{tr} of about 25%.

The products created in the intersection volume of the beams are detected via surface ionization on a hot Re ribbon mounted in a separately pumped ultra high vacuum chamber (residual gas pressure below 10^{-8} mbar). A channeltron converts the ions desorbing from the Re

surface to electron pulses which are counted by a two channel scaler synchronized with the HF beam modulator. One scaler counts the signal and background, the other only the background pulses. The detected scattering intensity (signal) I_{tot} is then derived as difference of the two scaler contents. Angular distributions of the signal $I_{\text{tot}}(\Theta)$ are obtained by rotating the main detector automatically around the intersection volume in the plane of the beams within a wide range of laboratory (LAB) scattering angles Θ . Crucial for the data analysis (see below) is the knowledge of time-of-flight (TOF) distributions of scattered particles at various scattering angles. They are measured employing a fast spinning chopper wheel with 8 equally spaced slots (2 mm wide) mounted between the skimmer of the HF beam and the scattering volume (see Fig. 1). The length of the flight path is 254 mm.

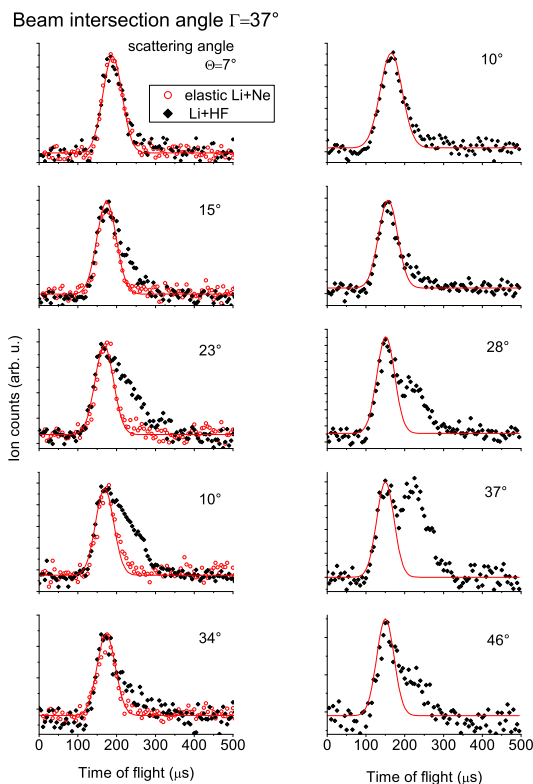


FIG. 2: Typical TOF profiles measured at $\Gamma = 37^\circ$ and 50° for the indicated scattering angles. The profiles are used to separate elastic (smooth curves) from the detected scattering intensity (data points). See text for more details.

The surface ionization is not specific with respect to alkali atoms or alkali compounds and detects both species with roughly the same efficiency. Therefore, the detected scattering intensity I_{tot} is proportional to the sum of fluxes of both the elastically scattered Li atoms I_{Li} and the products LiF, I_{LiF} . To separate both components we employ

the TOF distributions; examples are displayed in Fig. 2 for $\Gamma = 37^\circ$ and 50° . All TOF profiles feature a peak at short flight times and a broad shoulder or even a second peak at longer times. At $\Gamma = 90^\circ$ and higher Li velocities the peaks are always well separated [35].

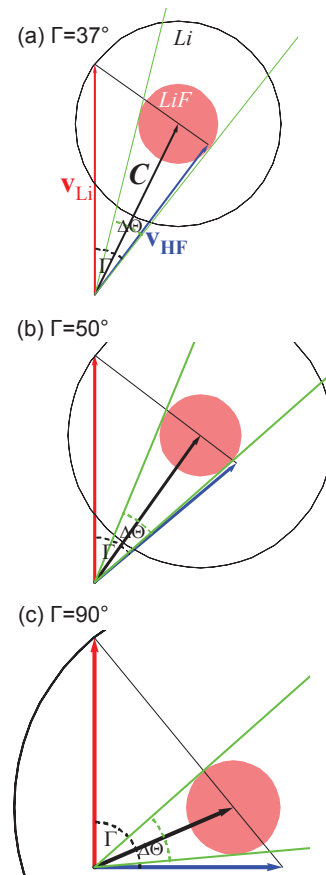


FIG. 3: Newton diagrams illustrating the kinematics for three beam intersection angles. The radius of the outer circle around the tip of the centroid velocity vector \mathbf{C} corresponds to the velocity of the elastically scattered Li atoms in the CM system, the radius of the inner filled circle to the maximal product velocity.

The collision kinematics are illustrated in Newton diagrams (Fig. 3) relating the LAB and center-of-mass (CM) frame velocities of reactants and products for beam intersection angles $\Gamma = 37^\circ$, 50° , and 90° . The light arrows represent the laboratory frame velocity vectors \mathbf{v}_{Li} and \mathbf{v}_{HF} of the reactants Li and HF which include the intersection angle Γ . The radius of the outer circle around the tip of the centroid velocity vector \mathbf{C} corresponds to the velocity of the elastically scattered Li atoms in the CM system, the radius of the inner shaded circle represents the maximal product velocity. The light straight lines that are tangent to the inner circle indicate the range of scattering angles $\Delta\Theta$ where reaction products LiF are expected to occur in addition to elastically scattered Li atoms. Elastically scattered Li atoms along \mathbf{C} have higher speeds than the LiF products and will there-

fore reach the detector at shorter flight times. Li atoms that are elastically scattered in the opposite direction in the CM frame have low speeds in the LAB frame and will spatially disperse on their way to the detector such that no significant contribution to the signal is expected.

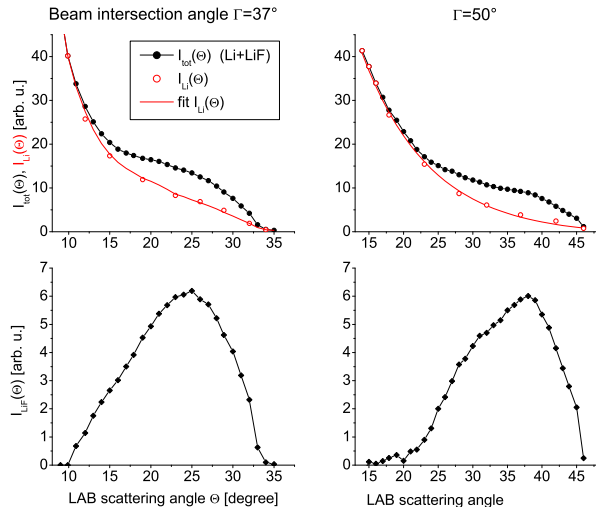


FIG. 4: Angular distributions of the detected (upper diagrams) and of the product (lower diagrams) scattering intensity measured at $\Gamma = 37^\circ$ and 50° . The open circles in the upper diagrams mark the elastic intensity deduced from the TOF distributions of Figure 2. The solid line is the best fit interpolation used to deduce the reactive scattering intensity (lower diagrams) by subtracting the elastic from the detected scattering intensity.

Thus, in Fig. 2 the peak at short flight times (fast particles) is attributed to elastically scattered Li atoms while the one at later times (slow particles) is associated with reaction products LiF. The solid line represents a numerically simulated TOF-distribution of elastically scattered Li atoms whose reliability was confirmed by a comparison with TOF profiles measured for the pure elastic system Li+Ne that features practically the same kinematics as Li+HF (open circles in Fig. 2). The elastic TOF profile is then fitted to the fast slope of the data. The area below this scaled elastic peak over the area below the entire TOF profile eventually provides the fraction of the detected scattering intensity associated with elastically scattered atoms. For a given Γ this fraction has been determined at scattering angles for which TOF distributions are available and used to isolate the angular distribution of the elastic component $I_{\text{Li}}(\Theta)$ from the detected scattering intensity $I_{\text{tot}}(\Theta)$. The result of this procedure is shown in Fig. 4 (upper panel). The open circles represent the angular distribution of the elastic component $I_{\text{Li}}(\Theta)$ and the solid line is a best fit curve through these points. The difference between the detected scattering intensity and the elastic component eventually yields the angular distribution of the product flux $I_{\text{LiF}}(\Theta)$ (lower

panel in Fig. 4). For more details see [35].

In principle the signal contribution identified with reactive scattering could also be generated by rotationally inelastic collisions. At $\Gamma = 50^\circ$ inelastic collisions $\text{Li} + \text{HF}(j = 0) \rightarrow \text{Li} + \text{HF}(j = 5)$ would yield Li atoms with similar CM speeds as the LiF products. At $\Gamma = 37^\circ$, Li atoms could be generated at speeds similar to those of LiF in inelastic collisions $\text{Li} + \text{HF}(j = 0) \rightarrow \text{Li} + \text{HF}(j = 3)$. Such selective rotation-changing collisions appear quite implausible, though, given the common scaling laws that predict a fast decay of the rotational inelastic collision cross section with increasing level spacing [40].

III. RESULTS

The IRCS, $\sigma_r(E_{\text{tr}})$, is proportional to the total flux of products $\dot{N}_{\text{LiF}}^{\text{total}}$ generated in the scattering volume \mathcal{V} and defined by the expression

$$\sigma_r(E_{\text{tr}}) = \dot{N}_{\text{LiF}}^{\text{total}} / (n_{\text{Li}} n_{\text{HF}} \bar{v} \mathcal{V}). \quad (4)$$

Here, n_{Li} , n_{HF} and \bar{v} denote the number densities of the indicated beams at the intersection volume and the mean relative velocity, respectively. Deviating from our earlier study [35], we leave the operational conditions of the beam sources constant and vary only the intersection angle Γ . Thus both densities n_{HF} and n_{Li} are constant, \bar{v} can be easily deduced from the most probable beam velocities (eq. 1), and an inspection of the intersection geometry shows that $\mathcal{V} = \mathcal{V}_{90^\circ} / \sin \Gamma$ holds approximately. The crucial quantity $\dot{N}_{\text{LiF}}^{\text{total}}$ is not directly accessible in the present in-plane scattering experiment but can be deduced from the measured total in-plane product flux $I_{\text{LiF}}^{\text{in-plane}}$ using the formal expression

$$\dot{N}_{\text{LiF}}^{\text{total}} = \frac{\dot{N}_{\text{LiF}}^{\text{total}}}{I_{\text{LiF}}^{\text{in-plane}}} I_{\text{LiF}}^{\text{in-plane}}. \quad (5)$$

Inserting eq. 5 into eq. 4 and suppressing all constant quantities we obtain the expression

$$\sigma_r(E_{\text{tr}}) \propto \frac{\dot{N}_{\text{LiF}}^{\text{total}}}{I_{\text{LiF}}^{\text{in-plane}}} \sin \Gamma / \bar{v} I_{\text{LiF}}^{\text{in-plane}} \quad (6)$$

relating the measured quantities and the relative integral reaction cross section. The ratio of fluxes in eqs. 5 and 6 corrects for the fraction of products that miss the detector; it can be readily deduced from the relative differential reaction cross section (DRCS) in the center-of-mass frame. In a previous study [33] using perpendicularly intersecting beams we have measured the relative DRCS at 6 energies within the range $82 \text{ meV} \leq E_{\text{tr}} \leq 376 \text{ meV}$ and found that the ratio is constant with respect to the energy within an error margin of $\pm 4\%$ [35]. Unfortunately, a comparable extensive investigation of DRCSs is not yet available for the present low energy range. However, a preliminary analysis of the product angular distributions measured at $\Gamma = 37^\circ$ (24 meV) and 50° (45 meV)

indicates that from 119 meV [33] ($\Gamma = 90^\circ$) to 24 meV ($\Gamma = 37^\circ$) a transition from the forward/backward to a preferred sideways type DRCS occurs. Taking this into account we find for all data sets that the product of factors left to the in-plane flux in eq. 6 is constant within the band width $\pm 5\%$. In view of a forthcoming more sophisticated determination of the DRCS we suppress these small corrections and derive the relative IRCS from the data using the simplified relation

$$\sigma_r(E_{\text{tr}}) \propto I_{\text{LiF}}^{\text{in-plane}}. \quad (7)$$

We have measured three sets of angular distributions A, B, and C at various intersection angles for the beam parameters given in Table 1. The constancy of the operational conditions was checked carefully by measuring a reference angular distribution repeatedly during one run. The intersection angles range from 37° to 90° (A,B) and $48^\circ \leq \Gamma \leq 90^\circ$ (C) corresponding to the energy range $25 \text{ meV} \leq E_{\text{tr}} \leq 108 \text{ meV}$ (A,B) and $50 \text{ meV} \leq E_{\text{tr}} \leq 131 \text{ meV}$ (C). For each angular distribution of a given set we measured between four and six TOF-profiles to separate elastic and reactive scattering.

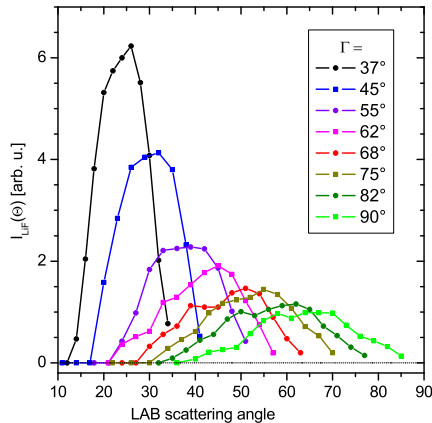


FIG. 5: Product angular distributions of data set A measured at the intersection angles 90° (open square), 82° (open circle), 75° (open triangle), 68° (open diamond), 62° (solid square), 55° (solid circle), 45° (solid triangle) and 37° (solid diamonds). Note the shift of the curves to smaller angles with decreasing Γ caused by the kinematics (Fig. 3) and the strong increase of the peak intensity. The area below the curves is the total product intensity used to determine the IRCS.

As an example we show in Fig. 5 the product angular distributions of set A. With decreasing Γ the curves shift to smaller LAB angles according to the changing kinematics (Fig. 3) and their peak intensities rise dramatically. The total in-plane intensity $I_{\text{LiF}}^{\text{in-plane}}$ or $\sigma_r(E_{\text{tr}})$ (eq. 7) is given by the sum over all product intensities multiplied by the Lab-angle increment (area below the curves),

$$I_{\text{LiF}}^{\text{in-plane}} = \sum I_{\text{LiF}}(\Theta_i) \Delta\Theta_i. \quad (8)$$

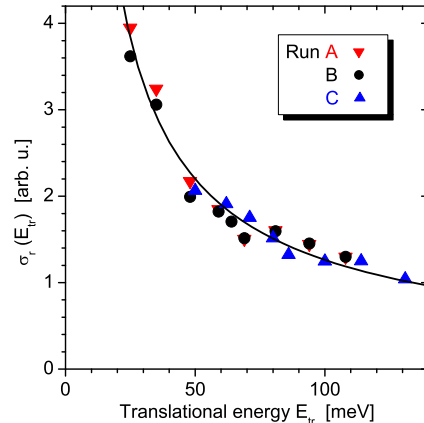


FIG. 6: The excitation function deduced from data set A (circles), B (triangles) and C (diamonds). The data sets are mutually normalized to obtain the best agreement within the overlap. The solid line through the data points is given by the simple power law $\sigma_r(E_{\text{tr}}) \propto (1/E_{\text{tr}})^{0.8}$.

The results for set A are compiled in Table 2 together with those for B and C and displayed in Fig. 6 as a function of the collision energy. The data points are normalized such that they agree optimally within the overlapping energy range. Their statistical error is not included in Fig. 6 for clarity. It can be estimated from the scatter of the points and amounts to about $\pm 5\%$ essentially due to uncertainties occurring in the process of separating elastic and reactive scattering. The solid line through the data points represents the simple power law $\sigma_r(E_{\text{tr}}) \propto (1/E_{\text{tr}})^{0.8}$.

IV. DISCUSSION

A strong motivation for performing the present experiments was the search for an answer to the question raised in the earlier study [35]: How does the excitation function continue below a collision energy of 82 meV? The previous results indicated two possibilities: either the excitation function assumes a maximum followed by a decline towards a threshold as one would expect for a reaction featuring a non-vanishing translational threshold energy or it continues to increase as expected for a reaction without threshold. The results of the present investigation strongly support the assumption that no threshold hinders the reaction of Li with HF. The excitation function continues to ascend monotonously at least down to 25 meV and is likely to continue this way [41]. Due to the elevated nozzle temperature of 500 K, required to suppress dimerisation, low rotational states of HF are populated with a mean rotational energy of 8.9 meV corresponding to a mean rotational quantum number of $\bar{j} = 1.4$ [35]. Thus the indicated threshold energies refer

TABLE II: Total in-plane scattering intensities in arbitrary units

E_{tr}/meV	Γ/degree	$J_{\text{LiF}}^{\text{in-plane}}$		
		A	B	C
25	37	83411	110104	
35	45	68510	93050	
48	55	45930	60628	
50	48			395200
59	62	39040	55431	
64	65		51909	
69	68	31774	46050	
71	60			335300
80	65			289750
81	75	31774	48590	
86	68			253200
94	82	30517	44170	
100	75			238650
108	90	27465	39540	
114	82			239200
131	90			199300

on average to the reaction $\text{Li}+\text{HF}$ ($v = 0, \bar{j}=1.4$). This internal energy may increase the threshold of the ground state reaction $\text{Li}+\text{HF}(v = 0, j = 0)$ on average by the mean rotational energy.

In Fig. 7 we have combined the results of the present and earlier experiments and obtain an excitation function that covers now a wide energy range of more than one order of magnitude from 25 meV to 376 meV. The curve can be subdivided into three sections: above 200 meV it is more or less constant, below 130 meV the function rises monotonously with decreasing E_{tr} , and in between it gradually changes the shape correspondingly. This behavior suggests the following classical reaction model.

(a) At energies > 200 meV a rigid sphere collision mechanism [34, 42] prevails where the reaction occurs with a constant, energy independent probability \mathcal{P} whenever the impact parameter b is smaller than the maximal one b_{max} . The resulting constant IRCS is then $\sigma_r = \mathcal{P}\pi b_{\text{max}}^2$. The mechanism neglects long range forces and thus all trajectories of the approaching reagents are straight lines.

(b) Below 130 meV long range forces start getting important. The force curbs the trajectories of the colliding reagents toward the center of the force and thus collisions with impact parameters larger than b_{max} may react. With decreasing energy the influence of the forces grows and thus the maximal impact parameter and the IRCS increase. Provided there is a vanishing threshold the IRCS continues to rise and eventually diverges classically for $E_{\text{tr}} \rightarrow 0$. Assuming that (i) the interaction potential energy is $\propto 1/R^s$ where R is the distance between

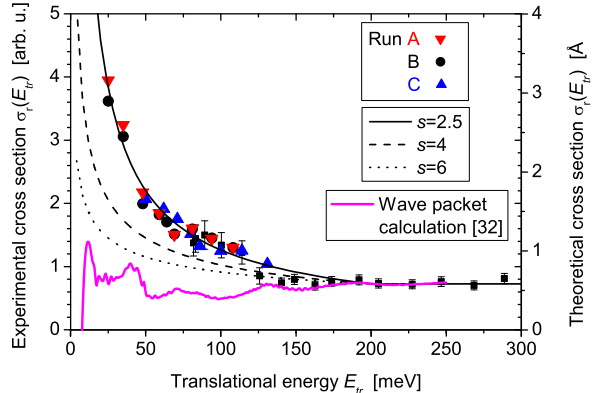


FIG. 7: Excitation function including the results of our previous study [35] (solid squares). The new and earlier results are mutually normalized to obtain the best agreement within the overlap. The curves at energies ≤ 200 meV are Langevin cross sections based on potential energy functions $\propto R^{-6}$ (dotted), $\propto R^{-4}$ (dashed) and $\propto R^{-2.5}$ (solid). The solid smooth line for energies ≥ 200 meV refers to a constant hard sphere collision model matched to the Langevin functions at 200 meV. The light solid line represents the result of recent wave packet calculations [32].

the reagents, and (ii) the reaction occurs with a constant probability whenever the reagents overcome the effective potential's maximum, then the IRCs is described by the "Langevin" power law $\sigma_r(E_{\text{tr}}) \propto (1/E_{\text{tr}})^{2/s}$ [34, 42]. The best fit curve in Fig. 6 corresponds accordingly to an interaction potential $\propto 1/R^{2.5}$. In Fig. 7 the $s = 2.5$ result (solid line) is compared with curves referring to $s = 6$ (dotted line) and $s = 4$ (dashed line) for energies below 200 meV. The corresponding potentials describe the long range forces of an atom-molecule ($s = 6$) and of an ion-molecule system ($s = 4$). Both curves feature the typical steep rise but are clearly at variance with our data. The best fit power $s = 2.5$ indicates that in our low energy range the chemical forces near the hard sphere radius are responsible for the rise of the IRCs rather than the asymptotic long range forces with $s = 6$.

(c) Between 130 and 200 meV the transition between the hard sphere and the potential energy dominated mechanism occurs.

The prediction of this classical model is illustrated in Fig. 7 as solid line where we have omitted the transition region and matched directly the hard sphere and Langevin functions at 200 meV. The curve recovers the data nearly quantitatively over this wide energy range.

The above classical model suggests a vanishing threshold but the experimental results provide only an upper boundary and a small threshold may well be in agreement with our findings. According to classical mechanics such a translational energy threshold is tightly related to the height of the potential energy barrier V_b separat-

ing reagents and products. Provided the approaching molecules are in their vibrational and rotational ground states ($v = 0, j = 0$) the formation of products requires that the translational energy of the approaching particles exceeds V_b . A non vanishing reaction threshold is then the consequence of an existing barrier.

Quantum mechanics relaxes the tight classical relation between threshold and barrier height. The colliding particles possess zero-point vibrational energy that varies during the approach adiabatically from the zero-point energy of the free molecule E_{vib}^0 to the one of the triatomic aggregate at the barrier E_b^0 . Taking this into account, product formation for ground state molecules ($v = 0, j = 0$) is then allowed in a classical sense, if the sum of the collision and zero-point energy of the reagent molecule exceeds the sum of the potential and zero-point energy at the barrier. The resulting semi-classical threshold energy

$$E_{\text{th}}^0 = V_b + E_b^0 - E_{\text{vib}}^0 \quad (9)$$

includes in addition to the barrier height V_b also the relevant zero-point energies E_b^0 and E_{vib}^0 . However, in contrast to classical mechanics, eq. 9 constitutes no rigorous lower limit for the translational energy leading to product formation. Due to quantum phenomena such as tunneling and resonances products may be formed also at collision energies far below this semi-classical threshold (see below).

To date all PESs available for Li+HF predict a significant barrier height V_b [6–16]. Including the zero point energy of HF (256 meV) and of the transition state (95 ± 10 meV depending on the geometric structure of the PES) the semi-classical threshold (eq. 9) for the most recent PESs amounts to 27 meV [12], 56 meV [15, 16] and 68 meV [13]. The present experiments provide as upper boundary for the threshold energy 25 meV and, considering the significant product flux observed for the Ar seeded Li experiment [41], 17 meV. Furthermore, the excellent fit of the data predicted by a model based on a vanishing threshold suggests a threshold located at energies $\ll 17$ meV. Thus our results suggest that the experimental threshold energy lies markedly below the predicted semi-classical values. This discrepancy could be due to insufficient accuracy of the computational methods used to calculate the PESs or to quantum effects that promote reactions at energies far below the semi-classical threshold. The latter is supported by recent wave packet calculations based on the PES of [15, 16] that predict a threshold for the total reaction cross section at about 10 meV which is qualitatively reconcilable with our measurements [32]. The

theoretical excitation function [32] is displayed in Fig. 7. The curve exhibits only a slight modulation around the value $\sigma_r \approx 0.5 \text{ \AA}$ as the translational energy is reduced down from $E_{tr} = 250$ meV to a threshold value of about 10 meV (see Fig. 7). The shape of the predicted excitation function departs significantly from the experimental one but the threshold energy is in accord with the present result. As the main source for product formation near threshold collisions with small J (total angular momentum) have been identified. The reaction probabilities for $J = 0$ exhibit a rich spectrum of oscillations and resonances as a function of energy [5, 32] but these structures disappear if realistic IRCs are calculated by summing over all J .

V. CONCLUSION

The benchmark reaction $\text{Li} + \text{HF} \rightarrow \text{LiF} + \text{H}$ has been studied at translational energies down to 25 meV using a new crossed-beam apparatus with variable scattering angle between Li and HF beams. This arrangement allows to tune the translational energy while keeping the beam source conditions constant. The integral reactive scattering rate (excitation function) is deduced from angle-resolved scattering as well as from time-of-flight traces in comparison with purely elastic Li+Ne scattering. The resulting excitation function, which extends earlier measurements to lower energies, steeply rises as the collision energy falls below about 150 meV. This behavior is consistent with a barrier-less Langevin-type reactive process with $R^{-2.5}$ -scaling of the atom-molecule interaction potential. Alternatively, an energy threshold below ~ 25 meV may be present as predicted by recent wave packet simulations [32].

Future efforts to further reduce the collision energy for conclusively disclosing or ruling out the existence of a reaction threshold will demand more sophisticated experimental approaches. To this end, a magneto-optical trap for preparing an ultracold Li scattering target is currently being set up and will be combined with a source for slow and cold molecules based on a rotating nozzle and electrostatic guiding [43].

Acknowledgments

Support from the Deutsche Forschungsgemeinschaft is gratefully acknowledged.

[1] N. Balakrishnan, J. Chem. Phys. **121**, 5563 (2004).

[2] R. V. Krems, Phys. Chem. Chem. Phys. **10**, 4079 (2008).

[3] M. T. Bell and T. P. Softley, Mol. Phys. **107**, 99 (2009).

[4] J. Hutson, **327**, 788 (2010).

[5] P. F. Weck and N. Balakrishnan, J. Chem. Phys. **122**, 154309 (2005).

[6] G. Balint-Kurti and R. Yardley, Faraday Disc. Chem. Soc. **62**, 77 (1977).

- [7] Y. Zeiri and M. Shapiro, *Chem. Phys.* **31**, 217 (1978).
- [8] Y. Shapiro and Y. Zeiri, *J. Chem. Phys.* **70**, 5264 (1979).
- [9] M. Chen and H. Schaefer, *J. Chem. Phys.* **72**, 4376 (1980).
- [10] S. Carter and J. Murrell, *Mol. Phys.* **41**, 567 (1980).
- [11] P. Palmieri and A. Laganà, *J. Chem. Phys.* **91**, 7303 (1989).
- [12] G. Parker, A. Laganà, and S. Crocchianti, *J. Chem. Phys.* **102**, 1238 (1995).
- [13] A. Aguado, M. Paniagua, M. Lara, and O. Roncero, *J. Chem. Phys.* **107**, 10085 (1997).
- [14] A. Jasper, M. Hack, D. Truhlar, and P. Piecuch, *J. Chem. Phys.* **116**, 8353 (2002).
- [15] R. Bobbenkamp, A. Paladini, A. Russo, H. Loesch, M. Menéndez, E. V. F. Aoz, and H.-J. Werner, *J. Chem. Phys.* **122**, 244304 (2005).
- [16] A. Aguado, M. Paniagua, and H.-J. Werner.
- [17] R. Walker, Y. Zeiri, and M. Shapiro, *J. Chem. Phys.* **74**, 1763 (1981).
- [18] A. Laganà, E. García, and O. Gervasi, *J. Chem. Phys.* **89**, 7238 (1988).
- [19] M. Baer, E. García, A. Laganà, and O. Gervasi, *Chem. Phys. Lett.* **158**, 362 (1989).
- [20] A. Laganà, X. Giménez, E. García, and O. Gervasi, *Chem. Phys. Lett.* **176**, 280 (1991).
- [21] M. Baer, H. Loesch, H.-J. Werner, and I. Last, *Chem. Phys. Lett.* **219**, 372 (1994).
- [22] M. Baer, I. Last, and H. Loesch, *J. Chem. Phys.* **101**, 9648 (1994).
- [23] G. Balint-Kurti, F. Gögtas, S. Mort, A. Offer, A. Laganà, and O. Gervasi, *J. Chem. Phys.* **99**, 9567 (1993).
- [24] F. Gögtas, G. Balint-Kurti, and A. Offer, *J. Chem. Phys.* **104**, 7927 (1996).
- [25] G. Parker, R. Pack, and A. Laganà, *Chem. Phys. Lett.* **202**, 75 (1993).
- [26] M. Lara, A. Aguado, O. Roncero, and M. Paniagua, *J. Chem. Phys.* **109**, 9391 (1998).
- [27] A. Laganà, R. Pack, and G. Parker, *J. Chem. Phys.* **99**, 2269 (1993).
- [28] W. Zhu, D. Wang, and J. Zhang, *Theor. Chem. Acc.* **96**, 31 (1997).
- [29] A. Laganà, A. Bolloni, and S. Crocchianti, *Phys. Chem. Chem. Phys.* **2**, 535 (2000).
- [30] A. Laganà, A. Bolloni, S. Crocchianti, and G. Parker, *Chem. Phys. Lett.* **324**, 466 (2000).
- [31] O. Höbel, R. Bobbenkamp, A. Paladini, A. Russo, and H. Loesch, *Chem. Phys. Lett.* **6**, 2168 (2004).
- [32] A. Zanchet, O. Roncero, T. González-Lezana, A. Rodríguez-López, A. Aguado, C. Sanz-Sanz, and S. Gómez-Carrasco, *J. Phys. Chem. A* **113**, 14488 (2009).
- [33] O. Höbel, Ph.D. thesis, Universität Bielefeld (2001).
- [34] M. Qiu, Z. Ren, L. Che, D. Dai, S. A. Harich, X. Wang, X. Yang, C. Xu, D. Xie, M. Gustafsson, et al., *Science* **311**, 1440 (2006).
- [35] O. Höbel, M. Menéndez, and H. Loesch, *Phys. Chem. Chem. Phys.* **3**, 3633 (2001).
- [36] S. Buntin, C. Giese, and W. Gentry, *J. Chem. Phys.* **87**, 1443 (1987).
- [37] Y. Hsu, J.-H. Wang, and K. Liu, *J. Chem. Phys.* **107**, 2351 (1997).
- [38] C. Naulin and M. Costes, *Chem. Phys. Lett.* **310**, 231 (1999).
- [39] H. Loesch and F. Stienkemeier, *J. Chem. Phys.* **98**, 9570 (1993).
- [40] K. Raghavan, S. K. Upadhyay, N. Sathyamurthy, and R. Ramaswamy, *J. Chem. Phys.* **83**, 1573 (1985).
- [41] In an experiment with an Ar seeded Li-beam we find at $\Gamma = 37^\circ$ and $E_{tr} = 17\text{meV}$ still a significant flux of products. However, we could not complete a full data set that overlaps with sets A and B.
- [42] R. Levine and R. Bernstein, *Molecular Reaction Dynamics and Chemical Reactivity* (Oxford University Press, New York, 1987).
- [43] M. Strebel, F. Stienkemeier, and M. Mudrich, *Phys. Rev. A* **81**, 033409 (2010).